Wear xxx (2009) xxx–xxx

Contents lists available at ScienceDirect

Wear

journal homepage: www.elsevier.com/locate/wear

Surface separation and contact resistance considering sinusoidal elastic–plastic multi-scale rough surface contact

W. Everett Wilson*, Santosh V. Angadi, Robert L. Jackson

Department of Mechanical Engineering, Auburn University, Auburn, AL 36830, United States

ARTICLE INFO

Article history:
Received 8 September 2008
Received in revised form 11 May 2009
Accepted 24 July 2009
Available online xxx

Keywords:
Rough surface contact
Multiscale
Contact mechanics
Electrical contact resistance
Contact area

ABSTRACT

The current work considers the multi-scale nature of surface roughness in a new model that predicts the real area of contact and surface separation as functions of load. This work is based upon a previous rough surface multi-scale contact model which used stacked elastic–plastic spheres to model the multiple scales of roughness. Instead, this work uses stacked 3D sinusoids to represent the asperities in contact at each scale of the surface. By summing the distance between the two surfaces at all scales, a model of surface separation as a function of dimensionless load is obtained. Since the model makes predictions for the real area of contact, it is also able to make predictions for thermal and electrical contact resistance. In accordance with concerns in previous works that the iterative calculation of the real contact area in multi-scale methods does not converge, this work not only tests but also gives conditions required for convergence in these techniques. The results are also compared to other existing rough surface contact models.

1. Introduction

There are many different methods to model the contact of rough surfaces including statistical [1–4], fractal [5–8], and multi-scale models [9–11]. The fractal mathematics based methods were derived to account for different scales of surface features not accounted for by the statistical models. The multi-scale models were developed to alleviate the assumptions imposed by fractal mathematics and to also improve how the material deformation mechanics are considered. This work uses a Fourier transform to convert the data into a series of stacked sinusoids, see Fig. 1. In a previous work [11] a method to calculate the surface separation from the multi-scale model was not provided. It is in the current work. In addition, this work differs from a previous multi-scale model [11] in that it uses sine shaped surfaces instead of spherical shaped surfaces to model contact of the asperities. The current work also provides a methodology for calculating the electrical and thermal contact resistance using the multi-scale methodology. This provides a method for including the effect of the scale dependent thermal properties [12–16]. Also, the surface characteristics necessary to obtain convergence of the iterative multi-scale scheme is examined.

There is also a great deal of previous work in the area of multi-scale contact. Archard [17] was probably the first to consider the multi-scale nature of surfaces in the modeling of the contact between them. By using a concept of multiple scales of asperities modeled as smaller and smaller spheres layed upon each other, Archard showed that a linear relationship between real contact area and load is obtained. This is of course very important in validating the sometimes experimentally observed Amonton's 'Law' of friction that friction is directly proportional to normal load. Much later, Ciavarella et al. [18] solved the contact problem of a 2D Weierstrass–Mandelbrot fractal surface in contact with a rigid flat using the same stacked asperity assumption. They modeled the surface deformation using the two-dimensional elastic sinusoidal solution given by Westergaard [19]. They also conclude that as higher scales are included in the contact model via fractal mathematics that the contact area will approach zero. This is a result of assuming that the surface is characterized by the W–M fractal.

Ciavarella et al. [20] also extended their 2D stacked model of contact between fractal surfaces by including a method to predict contact resistance and elastic contact stiffness (i.e. surface separation) from it. The methodology is very similar to that presented in the current work, except that the current work is for 3D surface contact, and the surface geometry is not assumed to be perfectly fractal. Rather, the current work uses experimentally measured surface profiles. Additional work on using 2D stacked multi-scale models to predict the contact resistance is given in ref [21].

In addition to the work by Jackson and Streator [11], Gao and Bower [22] also extended the multi-scale stacked contact model by including plastic deformation. The model by Gao and Bower also has similarities to the current work, especially that it is for 2D contact

* Corresponding author. Tel.: +1 205 566 8532; fax: +1 334 844 3307.
E-mail address: wilsowe@auburn.edu (W.E. Wilson).

0043-1648/$ – see front matter © 2009 Published by Elsevier B.V.
doi:10.1016/j.wear.2009.07.012

Nomenclature

a	Radius of the area of contact
A	Area of contact
$\bar{A}$	Individual asperity area of contact
A_n	Nominal contact area
B	Material dependent exponent
C	Critical yield stress coefficient
d	Separation of mean asperity height
D	Contact area factor
e_y	yield strength to elastic modulus ratio, S_y/E'
E	elastic modulus
E'	$E/(1-\nu^2)$
Er	electrical contact resistance
f	spatial frequency (reciprocal of wavelength)
F	constant found from slope of Fourier Series
G	asymptotic solution from JGH
H_G	geometrical hardness limit
H_c	heat capacity
k	thermal conductivity
K	hardness factor
Kn	Knudsen number
L	scan length
M	spectral moment of the surface
N	total number of asperities
p^*	average pressure for complete contact
P	contact force
$\bar{P}$	individual asperity contact force
$\bar{p}$	mean pressure
R	radius of hemispherical asperity
S_y	yield strength
T_r	thermal contact resistance
v_s	solid speed of sound
y_s	distance between the mean asperity height and the mean surface height
z	height of asperity measured from the mean of asperity heights

Greek symbols

α	coefficient of surface spectrum equation
δ	separation of mean surface height
γ	exponent of surface spectrum equation
η	area density of asperities
ρ	density of surface material
ρ_L	electrical resistivity of surface material
ρ_T	thermal resistivity of surface material
σ	standard deviation of surface heights
σ_s	standard deviation of asperity heights
λ	asperity wavelength
λ_{MFP}	phonon mean free path
Δ	asperity amplitude
Φ	distribution function of asperity heights
ω	interference between hemisphere and surface
ν	poisson's ratio

Subscripts

E	elastic regime
P	plastic regime
c	critical value at onset of plastic deformation
i	frequency level
JGH	from Johnson, Greenwood, and Higginson [10]
JG	from Jackson and Green [15]
asp	asperity
sur	surface
L	electrical
T	thermal
SD	scale-dependent

and the employed 2D elastic–plastic asperity contact model [23] appears to limit the contact pressure to 5.8 times the yield strength. The authors of the current work are not certain if that is always true for 2D elastic-perfectly plastic sinusoidal contact, but believe that the works by Krithivasan and Jackson [24], Jackson et al. [25] and Manners [26] show that for 3D elastic-perfectly plastic sinusoidal contact the pressure is not limited in this way.

Persson [27] also uses a diffusion theory to model rough surface contact. Persson's model is quite complex, but Pei et al. and Hyun et al. [28,29] were able to show a simplified version where it is proportional to the RMS slope of the surface. Pei et al. and Hyun et al. [28,29] also show that the model by Persson [27] appear to agree fairly well with deterministic finite element models. Ciavarella et al. [30] also constructed a discrete form of the Greenwood and Williamson model for contact of fractal surfaces which should in theory compare well to a full deterministic model. In contrast to Pei and co-workers [28,29] their results suggested that Persson's model will underpredict the real area of contact, and that the statistically based model by Bush et al. [31] makes a better prediction.

Additionally, Ciaverella et al. [32] made comparisons of their 2D multi-scale elastic stacked model to deterministic models, and also the model by Persson [27]. Interestingly, they also use a Fourier series to describe the Weierstrass fractal surface. Essentially, by using a Fourier series the scaling then becomes arithmetic instead of geometric. The current work also uses a Fourier series, but instead of for a perfectly fractal surface, it is for a experimentally measured surface profile. Ciaverella et al. [32] find that the 2D Persson and the multi-scale stacked model both appear to significantly underpredict the real area of contact. They also predict that the stacked model is only accurate if a very large fractal scaling parameter is used. It does appear that using a Fourier series in Persson's model improves the predictions of the model. They do not show results for the Archard type model using the Fourier series, which would then be more similar to the current work.

Again, the current work differs from the previous works because it uses a stacked multi-scale model based on the Fourier series obtained from an experimentally measured surfaces. In addition,

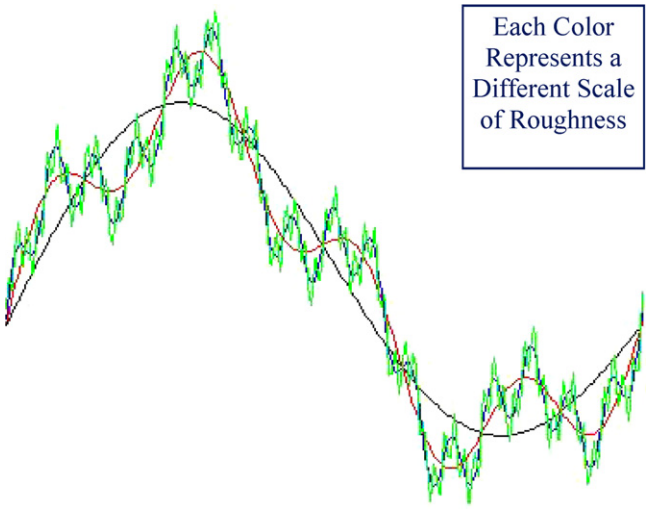

Fig. 1. A schematic depicting the decomposition of a surface into superimposed sine waves.

Please cite this article in press as: W.E. Wilson, et al., Surface separation and contact resistance considering sinusoidal elastic–plastic multi-scale rough surface contact, Wear (2009), doi:10.1016/j.wear.2009.07.012

3D sinusoidal asperity contact models are used for both elastic and elastic–plastic contact. Finally, the current work provides methodologies for making predictions of the surface separation and the contact resistance. In so doing, one apparent deficiency in the GW model regarding the prediction of the contact area to surface separation relationship is found and an approximate correction provided. In addition, an analysis is provided which shows when a stacked multi-scale model will converge to a non-zero real area of contact, rather than zero as occurs when the Weierstrass–Mandelbrot surface is used.

2. Methodology

2.1. Multi-scale perfectly elastic contact

The employed multi-scale model [11] uses the same direction of thought as Archard [33], but provides a method that can be easily applied to real surfaces. First, a Dektak 150 stylus profilometer was used to measure the surface data (although any profilometer could be used and the authors have also used other such sets of data in the model). Second, a fast Fourier transform is performed on the surface profile data. This series describes the surface as a summation of a series of sine and cosine waves. The complex forms of the sine and cosine terms at each frequency are combined using a complex conjugate to provide the amplitude of the waveform at each scale for further calculations. These amplitudes are then inserted directly into the stacked asperity model to describe each scale. Each frequency is considered a scale or layer of asperities which are stacked iteratively upon each other. All the scales from the Fourier series are used, such that the maximum frequency is related to the sample length and the minimum frequency is the Nyquist Limit. However, the current work finds that the smaller scales do not influence the calculated contact area. Therefore the resulting assumptions that are made by the current model are:

(1) Asperities are arranged so that asperities of smaller cross-sectional surface area are located on top of larger asperities. In the frequency domain this means that asperity distributions of higher frequencies are superimposed upon lower frequency asperities. This is similar to Archard's "protuberance upon protuberance" concept.
(2) Each "level" or frequency of asperities carries the same total load.
(3) The load at each frequency level is shared equally among all the asperities at that level.
(4) At a given frequency level, each asperity deforms according to a chosen elastic or elastic–plastic sinusoidal contact model, irrespective of the presence of higher frequency asperities upon it.
(5) A given frequency level cannot increase the contact area beyond what is experienced by the frequency level below it. This is now automatically enforced by the sinusoidal contact models, while in the original work [11] it was not because spherical contact models were used.

This differs from previous Archard-type multi-scale models [18,20–22,34] in that the current work does not assume that the surface follows a fractal structure exactly (such as the Weierstrass–Mandelbrot function). However, this results in the asperity scales not being geometrically scaled as far apart (this is one of the limiting assumptions of the model). In equation form these relationships are given by:

$$A = \left(\prod_{i=1}^{i_{max}} \bar{A}_i \eta_i\right) A_n \tag{1}$$

$$P = \bar{P}_i \eta_i \bar{A}_{i-1} \tag{2}$$

where A_r is the real area of contact, η_i is the real asperity density, P is the contact load, A_n is the nominal contact area, and the subscript i denotes a frequency level, with i_{max} denoting the highest frequency level considered. Note that $\eta_i = 2(f_i)^2$ because there are actually two sinusoidal asperity peaks for each square area of $1/f \times 1/f$.

Each frequency level is modeled using a sinusoidal contact model. Previously derived [11] equations fit to the data and asymptotic solutions given by Johnson, Greenwood, and Higginson [35] are used:

$$(A_{JGH})_1 = \frac{\pi}{f^2}\left[\frac{3}{8\pi}\frac{\bar{p}}{p^*}\right] \tag{3}$$

$$(A_{JGH})_2 = \frac{1}{f^2}\left(1 - \frac{3}{2\pi}\left[1 - \frac{\bar{p}}{p^*}\right]\right) \tag{4}$$

For $\bar{p}/p* < 0.8$

$$\bar{A}_i = (A_{JGH})_1\left(1 - \left[\frac{\bar{p}}{p^*}\right]^{1.51}\right) + (A_{JGH})_2\left(\frac{\bar{p}}{p^*}\right)^{1.04} \tag{5}$$

For $\bar{p}/p^* \geq 0.8$

$$\bar{A}_i = (A_{JGH})_2 \tag{6}$$

where p^* is the average pressure to cause complete contact between the surfaces of a single scale and is given by [35] as:

$$p^* = \sqrt{2}\pi E' \Delta_i f_i \tag{7}$$

This multi-scale model has been compared to other existing models in the previous work, but an additional comparison with a deterministic model is provided here. However, the comparison is only for a 2D version of the model that makes use of the Westergaard [19] solution of 2D sinusoidal contact. The 2D case is used to save computational time because deterministic models are computationally expensive. A 2D deterministic contact model is then constructed using the solutions found in Johnson [36] for a uniform pressure on a half-space, along with the theory of elastic superposition so that a non-uniform pressure distribution is modeled.

The resulting predictions of contact area versus load for the multi-scale and deterministic models are compared in Fig. 2 for surface 1 (which will be defined later in this work). Note that the deterministic model is more accurate for higher loads at which more nodes are in contact (this is also the region where it appears

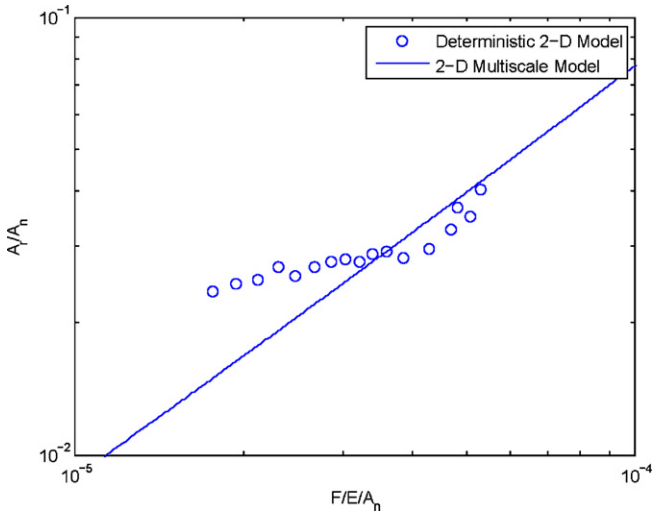

Fig. 2. Comparison of a 2D version of the multi-scale model with a deterministic model.

Please cite this article in press as: W.E. Wilson, et al., Surface separation and contact resistance considering sinusoidal elastic–plastic multi-scale rough surface contact, Wear (2009), doi:10.1016/j.wear.2009.07.012

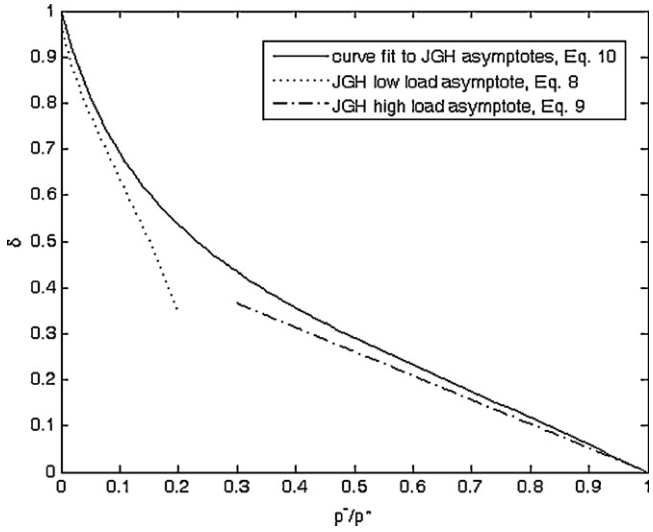

Fig. 3. Graphic depicting comparison of JGH asymptotic solutions with Eq. (10).

to compare best with the multi-scale model). Although, this is outside the immediate scope of this work, this comparison does show that the multi-scale model appears to compare fairly well with the deterministic model. It should be noted that this does not completely validate the model because the range of loads is small and the deterministic model also contains some numerical error and may not be completely accurate.

The current work also fits a new equation to the surface separation results given by JGH [35]. In previous works, the multi-scale model was used to relate area to load. However, for many applications it is also important to be able to predict surface separation. JGH gave asymptotic solutions for the surface separation. As $\bar{p}/p^*$ approaches zero, the solution is:

$$G_1 = 1 - \frac{1}{2}\left(3\pi^2 \frac{\bar{p}}{p^*}\right)^{2/3} + \left[4\ln(\sqrt{2}+1)\right]\left(\frac{\bar{p}}{p^*}\right) \tag{8}$$

While as $\bar{p}/p^*$ approaches 1 the solution given by [35] is:

$$G_2 = \frac{16}{15\pi^2}\left(\frac{3}{2}\right)^{3/2}\left[1 - \frac{\bar{p}}{p^*}\right]^{5/2} \tag{9}$$

In the current work an equation is then fit to join these two solutions:

$$\bar{\delta}_i = \Delta\left(1 - \frac{\bar{p}}{p^*}\right) \wedge \left(0.696\frac{\bar{p}}{p^*} + 0.158\right) \wedge (-0.847) \tag{10}$$

As seen in Fig. 3, Eq. (10) appears to be a good fit to the asymptotic functions given by Eqs. (8) and (9).

The separation height, H, between the two surfaces is calculated by subtracting the $\bar{\delta}_i$ value from the amplitude, Δ_i, at each scale level and then summing them together as follows (a graphical depiction of this method is shown in Fig. 4):

$$H = \sum_{i=1}^{i_{max}} (\Delta - \bar{\delta})_i \tag{11}$$

Note, that in the current work the surface separation is considering only the distance between the mean height of a rough surface and a smooth surface, as was originally done by Greenwood and Williamson. There are methodologies available in the literature to effectively combine two rough surfaces together to effectively model contact between them as contact between a smooth and rough surface.

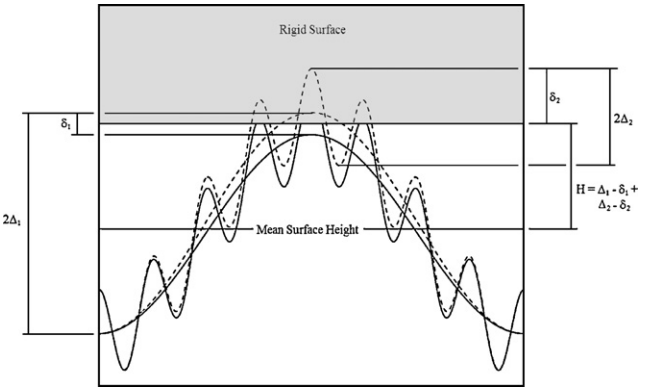

Fig. 4. Approximate schematic of a surface consisting of two scales in contact. Geometry is not to scale to improve clarity.

2.2. Multi-scale elastic–plastic contact

However, many of the asperities at the different frequency levels undergo plastic deformation. Therefore an elastic–plastic sinusoidal contact model is needed to consider this effect. The equations used in the current work to calculate the elastic–plastic contact are derived from FEM results by Krithivasan and Jackson [24] and Jackson et al. [25]. An alternative model was given by Gao et al. [23], but with differing results. Gao et al. found that the average pressure converged to $5.8S_y$ for high loads, while the analysis given by Krithivasan and Jackson [24] and Jackson et al. [25] found that the average pressure was not limited solely by S_y. The methodology is very similar to that of the perfectly elastic case with the exception that a different set of formulas is used once a calculated critical pressure is reached. The critical average contact pressure (P_c), critical average pressure over the nominal area ($\bar{p}_c$), the critical load and critical area (A_c) are given by:

$$P_c = \frac{1}{6\pi}\left(\frac{1}{\Delta f^2 E'}\right)^2\left(\frac{C}{2}S_y\right)^3 \tag{12}$$

$$A_c = \frac{2}{\pi}\left(\frac{CS_y}{8\Delta f^2 E'}\right)^2 \tag{13}$$

$$\bar{p}_c = 2A_c p_c f^2 = 2f^2\left(\frac{CS_y}{8\Delta f^2 E'}\right)^2 \frac{2}{\pi}\left(\frac{2CS_y}{3}\right) = \frac{1}{24\pi}\frac{(CS_y)^3}{(\Delta f E')^2} \tag{14}$$

where $C = 1.295\exp(0.736\nu)$.

At low loads, $P < P_c$, and consequently small areas of contact, it is acceptable to assume that any deformation of the asperities in contact will behave perfectly elastically. However, as load increases to the critical value, plastic deformation will begin to occur within the asperities. To evaluate the plastic deformation we replace Eq. (3) with:

$$A_P = 2(A_c)^{1/1+d}\left(\frac{3\bar{p}}{4CS_y f^2}\right)^{d/1+d} \tag{15}$$

$$d = 3.8\left(\frac{E'}{S_y}\Delta f\right)^{0.11} \tag{16}$$

This replacement results in the following equation for contact area at a single scale, i:

$$\bar{A}_i = (A_P)\left(1 - \left[\frac{\bar{p}}{p_P^*}\right]^{1.51}\right) + (A_{JGH})_2\left(\frac{\bar{p}}{p_P^*}\right)^{1.04} \tag{17}$$

Please cite this article in press as: W.E. Wilson, et al., Surface separation and contact resistance considering sinusoidal elastic–plastic multi-scale rough surface contact, Wear (2009), doi:10.1016/j.wear.2009.07.012

The pressure to cause complete contact during elastic–plastic deformation is then given by [25] as:

$$\frac{p_p^*}{p^*} = \left(\frac{11}{4\Delta/\Delta c + 7}\right)^{3/5} \tag{18}$$

where $\Delta c = \sqrt{2}S_y \exp(2\nu/3)/3\pi E' f$ and is the critical amplitude, below which the sinusoid will always deform in the elastic regime. Surface separation is calculated exactly as before by using Eq. (10), except the separation for pressures greater than $\bar{p}_c$ must have p^* replaced by p_p^*.

2.3. Statistical perfectly elastic contact

To compare and contrast the results of the multi-scale sinusoidal models, statistical contact models are also calculated using the same surface parameters and profilometer results. For the perfectly elastic case, this work employs the Greenwood and Williamson [1] approach for asperity contact. The GW method requires that a few crucial assumptions be made: (1) each asperity is assumed to behave independently of neighboring asperities, (2) all asperities have the same radius of curvature, (3) the asperity heights from the surface follow a Gaussian height distribution, and (4) only the actual asperity may deform, all substrate material is rigid as well as the contacting surface. See Appendix A for the equations used to model statistical perfectly elastic spherical contact in the current work.

2.4. Statistical elastic–plastic contact

Similar to the multi-scale model, some of the asperities will undergo plastic deformation as loads increase past the critical values. This work uses the methodology of Jackson and Green [37,3], referred to as JG for the remainder, which replaces the Hertzian contact solution in the GW model with equations suited for elastic–plastic deformation after critical values have been reached. For additional details on the methodology used for statistical elastic–plastic contact, please see Appendix B.

2.5. Electrical resistance

One of the concerns of this work is calculating the effect of surface roughness on electrical resistance. Therefore, the goal of this section is to determine how the flow of the current between surfaces is affected by the true area of contact for each load level. Since only a few, scattered asperities are actually in contact for any given load level, the current is restricted to very small contact patches when compared to the area of the entire surface. As the current flows through these asperity peaks, it will be effectively "bottlenecked" resulting in some resistance to the conduction as seen in Fig. 5.

Holm [38] gives a simple formula to calculate the electrical resistance due to asperity contact.

$$Er_{\text{asp}} = \frac{\rho_{L1} + \rho_{L2}}{4a} \tag{19}$$

where Er refers to the resistance value, a is the radius of contact, and ρ is the specific electrical resistance, or resistivity, of the respective surfaces. However, this equation is only good for a single asperity. In the case of both multi-scale and statistical techniques, additional equations are required to calculate resistance for the entire surface, (see the following sections).

2.6. Multi-scale electrical contact resistance

The multi-scale sinusoidal method presented here is an iterative method that calculates area and resistance for each particular frequency level. To predict electrical contact resistance, the first step is to calculate the average radius of contact per frequency level i:

$$a_i = \sqrt{\frac{A_i}{2\pi A_{i-1} f^2}} \tag{20}$$

Once the average contact radius is established, Eq. (19) is implemented to calculate resistance per asperity per level. For the sinusoidal case, it is assumed that the tip of the asperity is similar to a hemisphere so the radius of curvature at the tip is used. Oftentimes, an alleviation factor is used in thermal contact resistance calculations to account for the effect of a large contact radius, a, in relation to the asperity tip radius, R. Since electrical and thermal contact resistances are very mathematically similar, it stands to reason that the alleviation factor, Ψ, should also be included for electrical contact resistance. Though there are various ways to calculate this factor [39], the simplified version offered by Cooper et al. [40] is chosen for this work:

$$\Psi_i = \left(1 - \sqrt{\frac{A_i}{A_{i-1}}}\right)^{1.5} \tag{21}$$

The alleviation factor, Ψ_i, is combined with the resistance value and the result is summed over all possible iteration levels to find the total resistance for the entire surface in contact.

$$Er_{\text{total}} = \sum_{i=1}^{i_{\max}} \frac{\Psi_i Er_i}{\eta_i A_{i-1}} \tag{22}$$

It is important to note that this technique calculates the resistance for each frequency level and then sums them over all frequency levels to calculate the total. Another technique exists that only evaluates the resistance for the highest frequency level that still reduces contact area [41]. This alternative technique is not considered in this work. Also, the method does not change depending on the inclusion of plasticity since all resistance calculations are done after obtaining the contacting area.

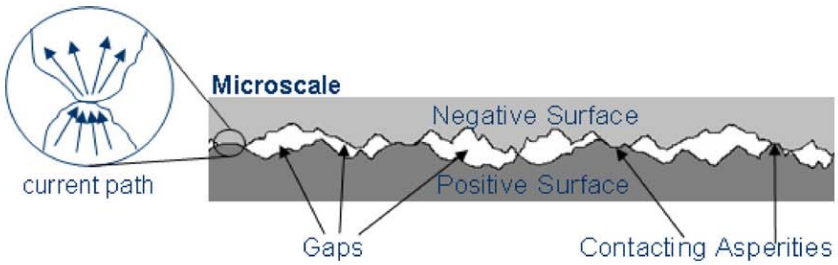

Fig. 5. Schematic of "bottlenecked" current flow through asperities.

Please cite this article in press as: W.E. Wilson, et al., Surface separation and contact resistance considering sinusoidal elastic–plastic multi-scale rough surface contact, Wear (2009), doi:10.1016/j.wear.2009.07.012

2.7. Statistical electrical contact resistance

To continue comparing the multi-scale results with that of the earlier statistical method (see Appendices A and B), the electrical contact resistance is also obtained for statistical perfectly elastic and elastic–plastic methods. Greenwood and Williamson [1] include a solution for conductance in their work. Resistance is simply the inverse of conductance so the technique for calculating perfectly-elastic contact resistance is as follows:

$$\frac{1}{Er_e(d)} = 2A_n\eta\Psi\rho_L^{-1}R^{1/2}\int_d^\infty \omega^{1/2}\Phi(z)dz \tag{23}$$

Note the inclusion of the alleviation factor, Ψ. The statistical method is not a multi-scale procedure so the alleviation factor is calculated as follows:

$$\Psi = \left(1 - \sqrt{\frac{A_r}{A_n}}\right)^{1.5} \tag{24}$$

Elastic–plastic statistical contact is calculated in the same manner except using a different elastic–plastic asperity contact model. One such technique is given by Kogut and Etsion [42], which is used as an outline for this work. However, there are dissimilarities since this work relies on the methodology of Jackson and Green [37]. Eq. (23) is still used but the contact radius, a, has changed in accordance with the work of Jackson and Green.

$$a_{ep} = \sqrt{D\omega R} \tag{25}$$

where if $0 \le \omega/\omega_c \le 1.9$, then $D = 1$, but if $\omega \ge 1.9\omega_c$, then $D = (\omega/1.9\omega_c)^B$.

By applying the contact radius in Eq. (25) to the resistance calculation in Eq. (23), the elastic–plastic electrical contact resistance is obtained.

$$\frac{1}{Er_{ep}(d)} = A_n\eta\Psi\int_d^\infty \frac{2a_{ep}}{\rho_L}\Phi(z)dz \tag{26}$$

Similar to the multi-scale model, the alleviation factor, ψ, is included here as well.

Additional details for the perfectly-elastic or elastic–plastic statistical electrical resistance calculations Eqs. (23–26) can be found in Appendices A and B.

2.8. Scale dependent thermal contact resistance

Thermal contact resistance refers to the build-up of heat at the boundary between the two surfaces due to the same "bottleneck" effect referred to in electrical resistance seen in Fig. 5. Technically, heat can flow across the gaps in the material as well as through the contacting asperities. However, the heat transfer across the gaps is neglected since like electrical current, usually the majority of the heat flow will follow the path of least resistance or in this case the asperities in contact. Indeed, thermal and electrical contact resistances are very similar effects and are computed using very similar methods as well.

Scale dependency is an emerging topic in the field of contact resistance. The concept behind scale dependency is that as a sample of a material is viewed at increasingly higher magnification the material properties actually change according to how small of a sample is viewed. The reason for this is that at some point one is viewing actual atoms pressed against each other instead of the continuous material. Therefore, at this point the scale is below that where most imperfections and features are seen, such as grain boundaries. This impacts the multi-scale contact model because it takes into account many different scales of asperities down to where this phenomenon is seen. To include these effects, the thermal contact resistance is replaced with a scale dependent value found in the work of Prasher and Phelan [43].

The current work finds that the inclusion of scale dependent single asperity thermal contact resistance does not affect the predicted overall thermal contact resistance significantly for the sinusoidal based multi-scale rough surface contact model. This is also confirmed for the different spherical based multi-scale contact model by [41]. Due to the similarity of electrical contact resistance, thermal contact resistance and scale dependent thermal contact resistance, the methodologies and results will not be included but can be seen in the work of Jackson, Bhavnani, and Ferguson [41] using a multi-scale spherical contact model.

3. Results

3.1. Convergence of real contact area

As mentioned previously, the data set used for this model is converted into a series of stacked sine waves using the Fourier Transform. All calculations for the model are then made based off the amplitude and wavelength of these sine waves. The multi-scale model considered here assumes that the predicted area converges as all scales are included in the model. This is important because if the predictions do not converge then the area will approach zero as smaller scales are included as was predicted by [18]. In order to test convergence, a power fit is found for the nominal amplitude as a function of wavelength.

$$\Delta_i = \alpha\lambda_i^\gamma \tag{27}$$

where λ_i is the wavelength (inverse of frequency) and both α and γ are constants derived by fitting Eq. (17) to the Fourier series of the surface data. For a particular surface the best fit was found with $\alpha = 0.085$ and $\gamma = 1.5$. Starting with this "benchmark case", the values α and γ are then varied individually to find any critical values at which point convergence is not possible. This process is carried out for both perfectly elastic and elastic plastic cases.

The first test of convergence is to see the role that α plays in Eq. (27). For this test, α ranges from 10^{-3} to 10^3 by an order of magnitude at each step. The fit value for α was found to be 0.085, which falls within the range of values tested. As seen in Figs. 6 and 7, α does not appear to play a significant role in convergence since all the lines show a flattening trend at the smaller wavelengths. This

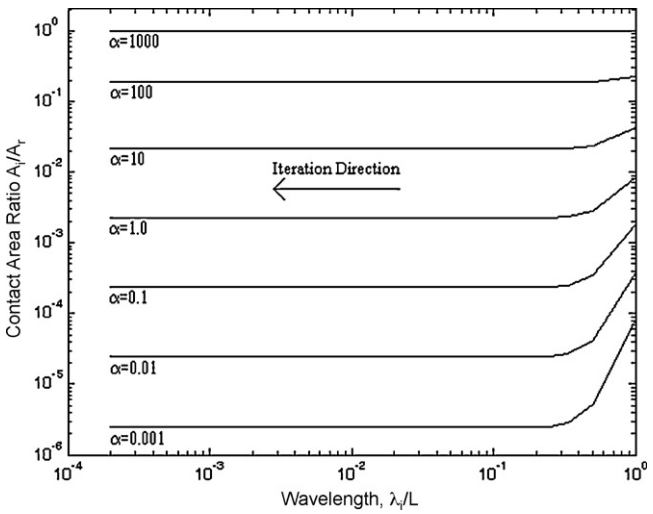

Fig. 6. Contact area ratio as a function of wavelength for perfectly elastic multi-scale method where α is varied in Eq. (27).

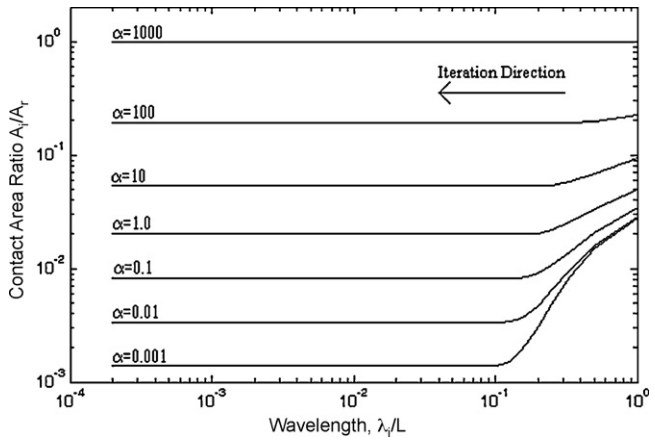

Fig. 7. Contact area ratio as a function of wavelength for elastic–plastic multi-scale method where α is varied in Eq. (27).

result is independent of plasticity since the same trend is seen in both Figs. 6 and 7.

The second test of convergence is conducted by varying the value of γ in Eq. (27). The results from this test (shown in Figs. 8 and 9) show that this exponent is the deciding factor for convergence in both perfectly elastic and elastic–plastic cases. For this test γ is varied from 0 to 2 at intervals of 0.25. For a good fit to the FFT data, γ was found to be 1.5, which is within the range of values tested. γ values lower than 1 show a continual slope despite the wavelength size suggesting that convergence is not possible for these cases. This result is shown to be similar for both perfectly and elastic–plastic cases.

The results of these tests have shown that convergence is dependent upon the exponent, γ, in the power function fit to the FFT data in Eq. (27). As the scales are iteratively included, the contact area reduces. Therefore, the average pressure continues to increase and may eventually become larger than the pressure to cause complete contact (p^*). If this pressure stays above the pressure to cause complete contact (p^*) the area will no longer reduce and convergence is obtained. Therefore, for convergence to occur, p^* must stay constant or decrease as λ decreases. This suggests that the requirement for convergence depends upon the following relationship:

$$p^* \propto \frac{\Delta}{\lambda} = \alpha\lambda^{\gamma-1} \tag{28}$$

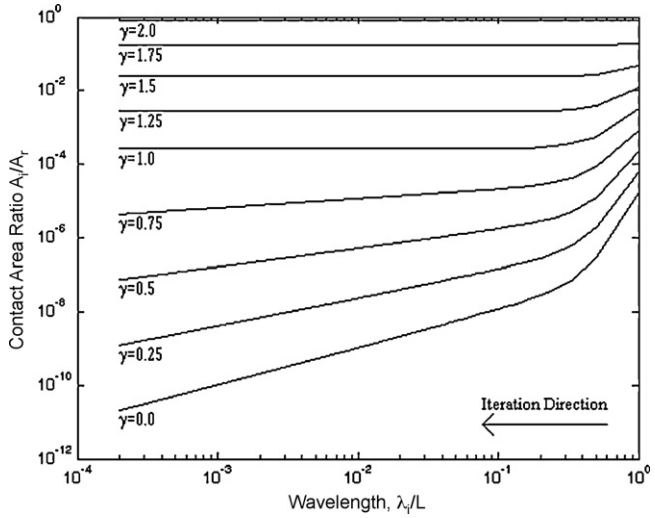

Fig. 8. Contact area ratio as a function of wavelength for perfectly elastic multi-scale method where γ is varied in Eq. (27).

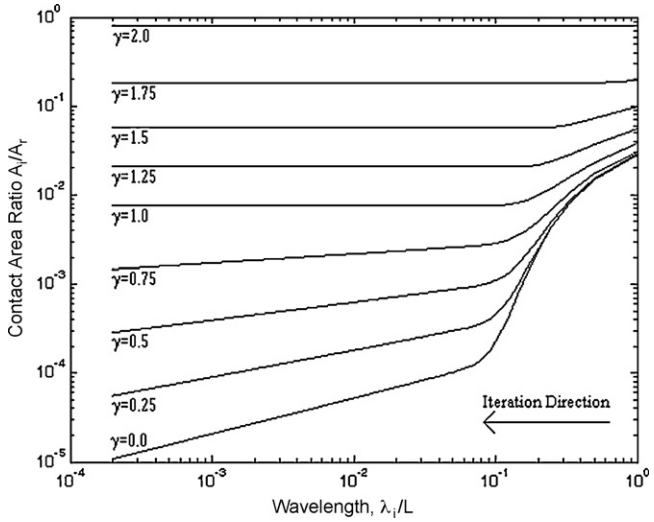

Fig. 9. Contact area ratio as a function of wavelength for elastic–plastic multi-scale method where γ_2 is varied in Eq. (27).

As long as Δ/λ stays constant or decreases as λ decreases then the multi-scale sinusoidal method will converge. This condition is met as long as the γ value in Eqs. (27) and (28) are greater than or equal to 1, as shown by Eq. (28).

3.2. Model predictions

This work assumes realistic material properties for all results gathered (see Table 1). Since this work includes an examination of electrical resistance, the material of choice is Tin due to its common use in electrical connectors and circuits. The surface profile is measured from machined metal samples using a stylus profilometer. A scan length of 400 μm was used. To ensure an accurate comparison of the contact models, the material properties and surface geometry are kept constant for all calculations. For actual calculations, Matlab™ is used for evaluating mathematical results.

Once the data is gathered, a Fast Fourier Transform is performed as mentioned before. All frequencies present in the surface data are included. This means that the minimum frequency was based on the scan length and the maximum frequency was the Nyquist Limit. However, we found that the higher frequency (smaller scale) asperities did not contribute anyway because they just flatten out under high pressures. The result is then converted to amplitude via the complex conjugate. Then multi-scale models can be calculated as described above. For the GW and JG models, the statistical parameters are acquired using McCool's [44] methods by finding the spectral moments about the surface (see Appendix B). From here, the GW model is fairly straightforward except for the integrals found in Eqs. (23), (26), (35) and (36). To solve these, numerical integration techniques are employed. Simpson's Method is used by first breaking the integral into 1000 sub-intervals and performing the Simpson's interpolation on each subinterval.

As seen in Fig. 10, higher loads result in a greater area of contact for the two surfaces. The comparison of the two modeling techniques resulted in good qualitative agreement but poor quantitative agreement. Greater contact area also results from the inclusion of plastic deformation. This is caused by the behavior of the solid asperities to flow and flatten under plastic deformation.

Table 1
Material properties of tin.

$Sy = 14 \times 106$ Pa	$E = 41.369 \times 109$ Pa
$\rho_L = 11.5 \times 10{-}8\ \Omega$ m	$\nu = 0.36$

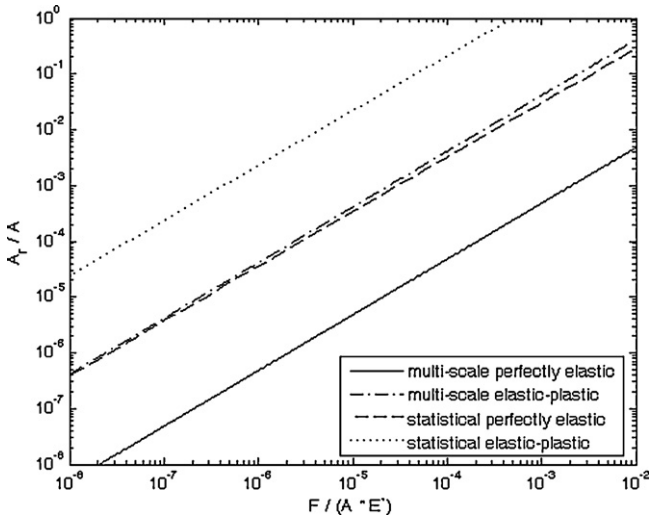

Fig. 10. Plot of non-dimensional area vs. load.

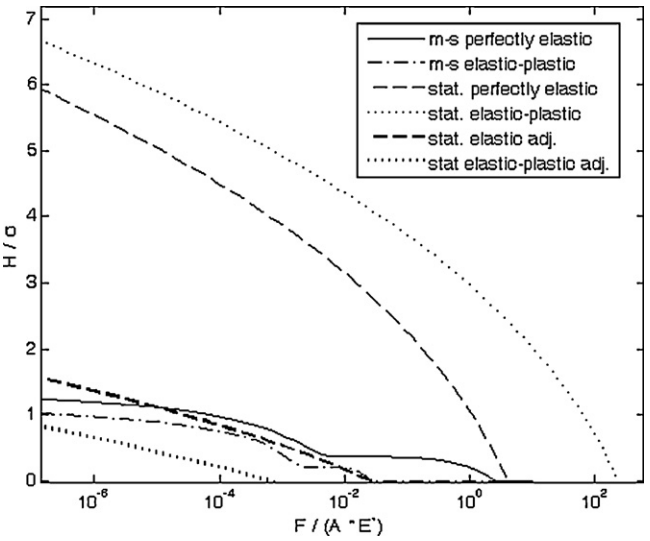

Fig. 13. Plot of non-dimensional surface separation vs. load.

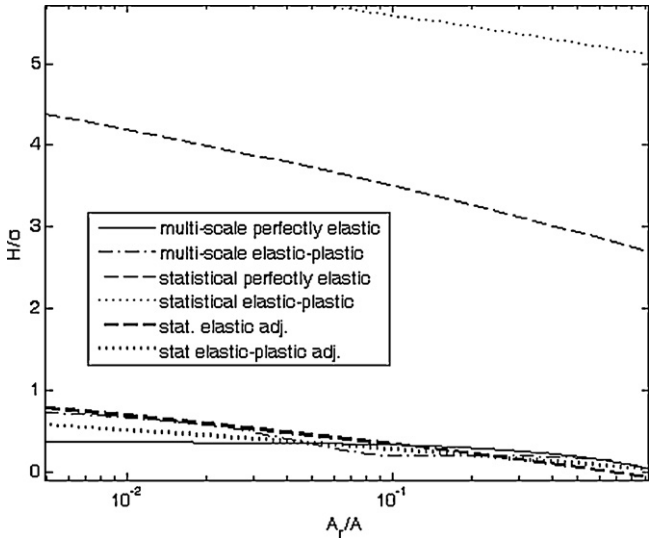

Fig. 11. Area compared to Surface Separation including the adjusted separation for Statistical Contact Methods.

The asperity material tends to "flow" resulting in greater deformation as well as "filling in" the low spots around each asperity. This combines with the higher loads to produce larger amounts of contact. These two techniques are calculated in very different manners using almost no common equations. Therefore, this qualitative agreement serves to confirm the accuracy of the trends of both methods for modeling the contact of rough surfaces.

Fig. 11 shows the surface separation as a function of the calculated real area of contact. Although the overall trends of the two models are similar, the calculations for the statistical methods both show the separation reaching zero before the surfaces are in full contact. Logically, when contact is complete, the real area of contact should be at its maximum and surface separation should be zero. The reasons for difference amongst the statistical and multi-scale methods are three-fold. First, in the multi-scale method, all asperities are loaded equally so they may actually be over-compressed. Second, the statistical model does not consider the interactions between adjacent asperities. At some loads, the valleys neighboring each peak may be rising as they fill in with the plastically deformed material. Third, and what the authors believe is the most important, the statistical method does not adjust the mean height based on asperity deformation.

Also, the sharp elbows seen in the curves are believed to be an artifact of the multi-scale modeling technique resulting from the flattening of scales which then no longer influence the solution.

$$\delta_{\mathrm{ADJ}} = \frac{\delta + 0.5\beta\sigma}{2} \tag{29}$$

As seen in Fig. 12, Eq. (29) takes the average of the mean surface height at zero deformation, $\beta\sigma/2$, and the distance from the mean surface height to the peak of the deformed surface, δ. The β value is found not to be constant and varies not only for different surfaces but also depends on whether plasticity is considered. As shown in Fig. 12, $\beta\sigma$ represents the peak to valley height of the surface. Since statistically 68% of the asperities are accounted for between -2σ and 2σ and 99.7% accounted for between -6σ and 6σ, one could make an approximation of β between 4 and 12. For the surface data considered in the current analysis a value of $\beta = 5.2$ was found to work well for the perfectly elastic case. However, for elastic–plastic deformation, $\beta = 10.02$ produced the appropriate results. These adjustments will be different for each case because

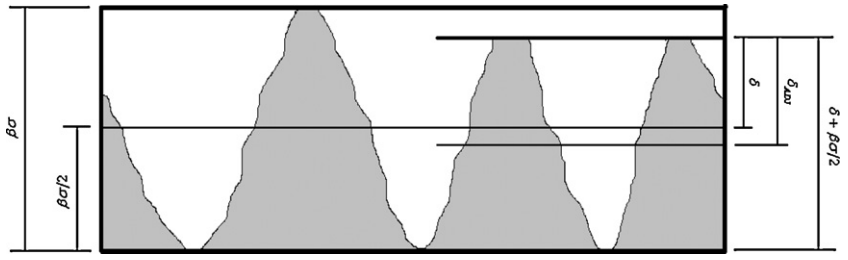

Fig. 12. Graphical comparison of surface separation and adjusted surface separation.

Please cite this article in press as: W.E. Wilson, et al., Surface separation and contact resistance considering sinusoidal elastic–plastic multi-scale rough surface contact, Wear (2009), doi:10.1016/j.wear.2009.07.012

the amount of compression and deformation will be different for the perfectly elastic and elastic–plastic cases. The resulting adjusted statistical model results are shown in Fig. 11.

Fig. 13 shows, as expected, that greater loads as well as plastic deformation serve to decrease the gap between the surfaces. This is logically correct since greater loads increase the area of contact through deforming the asperities. One would expect the flattening of the asperities to allow the surfaces to come closer to each other and eventually contact completely when the calculated area is equal to the nominal area. The adjustment given by Eq. (29) once again improves the agreement between the statistical and multi-scale methods.

Perhaps surprisingly, the models predict similar results on the same order of magnitude. Once again the overall trends of both the statistical and multi-scale methods are confirmed by one another. In this case though, the estimated behavior of the separation is fairly different. Both methods show the decreasing gap with greater loads but they follow significantly different curves.

Without strong experimental confirmation, it is difficult to ascertain the accuracy of either model. However, the current multi-scale model will result in larger contact stiffness than predicted by the statistical models. Stiffness is defined as the change in contact force per change in surface separation. This appears to agree with experimental findings by Drinkwater et al. [45] using acoustic methods.

3.3. Electrical contact resistance

For the particular case of modeling the contact of an electrical connector, one concern was the amount of electrical resistance due to the "bottleneck" effect of contacting asperities. Fig. 14 shows the calculated results for this effect and compares the results for the multi-scale and statistical models described here. Since the electrical resistance is due to the gaps between the surfaces, it follows naturally that the electrical resistance decreases with load which as expected is inverse to the behavior of contact area. Yet again, the greater contact area at lower loads seen by the elastic–plastic cases shows in the electrical resistance plot as these cases decreases in resistance considerably quicker than the elastic cases. The multi-scale and statistical models also agree surprisingly well even though they make different predictions for contact area. This suggests that it can be difficult to validate these models based on contact resistance measurements alone. Interestingly, the ECR appears to decrease rapidly as complete contact is approached (as seen by the elbows at the end of each curve).

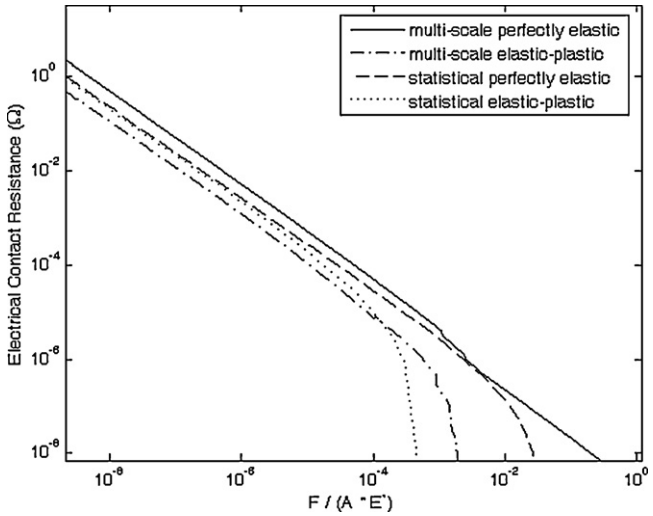

Fig. 14. Electrical contact resistance as a function of non-dimensional load.

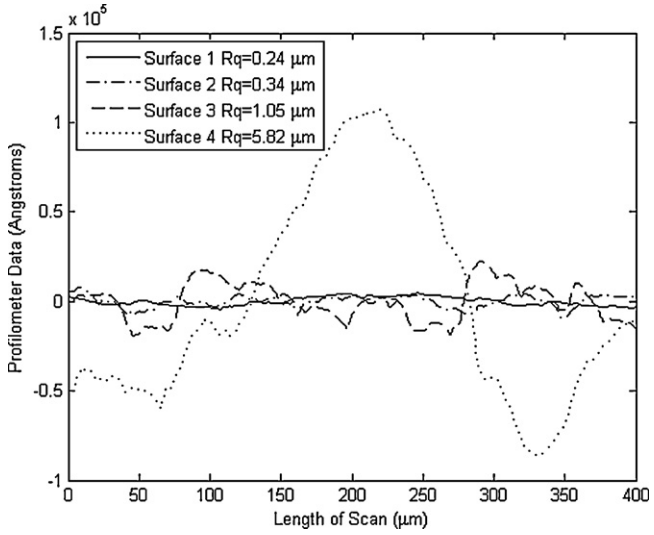

Fig. 15. Surface profile data with different roughness values.

Table 2
Rough surface characteristics and convergence variables.

Surface	Roughness (μm)	α in Eq. (27)	γ in Eq. (27)	RMS error of FFT to Fit
1	0.24	0.13	1.60	0.3322
2	0.34	0.085	1.5	0.4134
3	1.05	0.037	1.4	0.4053
4	5.82	0.006	1.0	0.0678

3.4. Comparison between multiple surfaces

The next concern is what effect real multi-scale roughness plays in the contact area, separation, and resistance for different surfaces. To measure this effect, multiple surface profiles were obtained using a stylus profilometer on four surfaces with roughness varying from 0.24 μm up to 5.82 μm. Fig. 15 shows that the smoother profiles are relatively flat where the roughest shows rather large changes in surface heights.

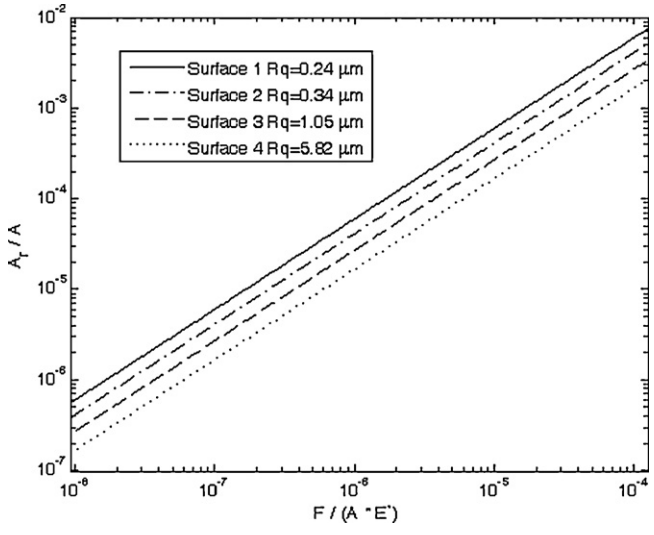

Fig. 16. Real area of contact as a function of dimensionless load for surfaces of different roughness.

Please cite this article in press as: W.E. Wilson, et al., Surface separation and contact resistance considering sinusoidal elastic–plastic multi-scale rough surface contact, Wear (2009), doi:10.1016/j.wear.2009.07.012

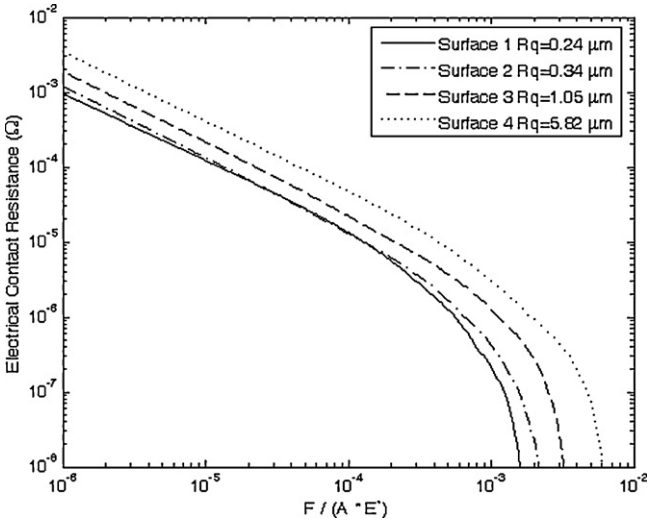

Fig. 17. Electrical contact resistance (ECR) as a function of dimensionless load for surfaces of different roughness.

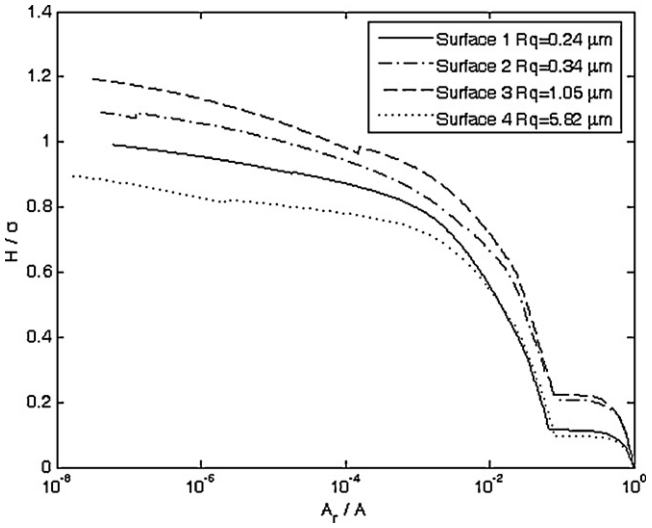

Fig. 19. Surface separation as a function of real area of contact for surfaces of different roughness.

Table 2 provides a comparison between roughness and the power equation, Eq. (27), fit to the Fourier transform for each of the four surfaces examined in this work. The root-mean-square error between the fit and FFT data is given as well. Some of the error values are quite high due to the scattering of the FFT data which does not allow for a precise fit. In application, this could result in large differences in the model predictions when a power equation is used versus the actual data. In the current work the actual data is used in the multi-scale model. It is important to note that the values for α vary seemingly independent of roughness whereas γ behaves inversely of roughness. Therefore, the roughest surface has $\gamma = 1.0$ which is at the limit of convergence as seen in Figs. 8 and 9. Therefore there may be some very rough surfaces for which the multi-scale technique will not converge. This is not a concern for relatively smooth surfaces however.

As seen in Fig. 16, the real area of contact changes, but remains in the same orders of magnitude despite the different roughness values of the four profiles. This results in the predicted real area of contact being extremely similar despite the change in roughness between surfaces. However, as is expected, the graph does show that the results are ranked in order of decreasing roughness with smoother surfaces showing a greater contact area for each load level.

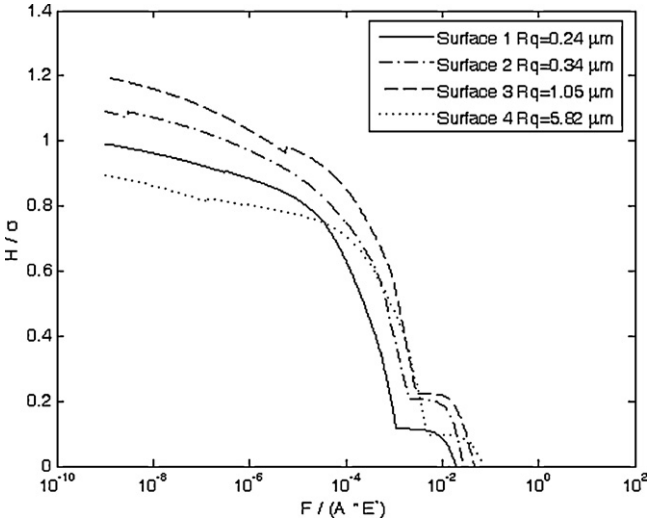

Fig. 18. Surface Separation as a function of dimensionless load surfaces of different roughness.

In accordance with the real area of contact, electrical contact resistance is very similar for the four surfaces and is also ranked according to roughness with the smoothest surface having the least resistance values as seen in Fig. 17. The electrical contact resistance shows the inverse trend between the surfaces as the contact area until high loads are reached.

Fig. 18 shows some interesting results when considering different surface roughness. The surfaces rank themselves according to roughness again where the smoothest surface has the lowest separation. This is true except for surface 4, the roughest, which has broken rank for low loads. However, as higher loads decrease separation the roughest surface does in fact require a greater force than the others to reach zero separation. Although surface 4 is rougher, the differences in behavior may be caused by a different surface structure unique to #4 that the others don't share.

Fig. 19 shows the relation of surface separation with the real area of contact. In this case the same behavior is seen as in Fig. 18, but the limiting situations of the multi-scale model are very apparent in this plot. The multi-scale method predicts surface separation to reach zero as full contact approaches. This is shown at $A_r/A = 10^0 = 1$, where the results seem to be sharply cut off so that the logical condition of zero separation at full contact is upheld.

4. Conclusions

The results from a multi-scale model based on stacked sinusoidal surfaces have shown to be qualitatively similar in comparison with existing statistical contact models. When viewing surface separation as a function of dimensionless load, it seems that the multi-scale models offer a differing description of how the surface behaves. At high loads, the multi-scale methods predicts no separation between the surfaces which correlates exactly with the area of contact equaling the apparent area of contact (complete contact). However, even though the statistical methods show a similar trend as the maximum area is reached, there appears to still be some separation between the two surfaces. This is most likely a result of the statistical methods being designed more for lightly loaded contacts and ignoring the change in overall peak to valley height between asperities at higher loads. The adjusted statistical model separation calculation offered in this work takes this effect into account and does show zero separation at the maximum con-

Please cite this article in press as: W.E. Wilson, et al., Surface separation and contact resistance considering sinusoidal elastic–plastic multi-scale rough surface contact, Wear (2009), doi:10.1016/j.wear.2009.07.012

tact area. Electrical contact resistance predictions seem reasonable based on the similarity between statistical and multi-scale methods. Actually, the statistical and multi-scale models predict very similar values, while the predicted contact areas are not as similar. This suggests that using contact resistance measurements may not be an effective way of evaluating rough surface contact models.

In response to concerns about the convergence of the multi-scale techniques, this work relates a power fit to the FFT data which reveals that the sinusoidal multi-scale technique will converge as long as the average pressure stays constant or decreases as the wavelength decreases. This situation requires that the exponent in the power fit remain 1 or greater for the multi-scale sinusoidal technique to converge.

Finally, once the multi-scale sinusoidal method is verified as a valid contact model, results for a variety of real surfaces shows the overall expected trends for area, electrical contact resistance and surface separation. As is expected, the results for the surfaces are ranked according to roughness yet produce extremely similar results. Upon first inspection, it appears that surface separation does not match the ranking behavior for the various surfaces. However, at greater loads, lower roughness values do decrease surface separation.

Appendix A. Statistical elastic model

Using the Greenwood and Williamson type statistical method hinges upon obtaining statistical parameters that describe the surface. The radius of curvature, R, and the areal asperity density, η, are calculated by McCool [45] using the spectral moments of the surfaces:

$$M_2 = \frac{1}{N}\sum_{n=1}^{N}\left(\frac{dz}{dx}\right)_n^2 \tag{30}$$

$$M_4 = \frac{1}{N}\sum_{n=1}^{N}\left(\frac{d^2z}{dx^2}\right)_n^2 \tag{31}$$

where N is the total number of asperities on the surface and z is the distance from the mean height of the surface to the asperity peak. Then R and η are found from:

$$\eta = \left(\frac{M_4}{M_2}\right)\left(\frac{1}{6\pi\sqrt{3}}\right) \tag{32}$$

$$R = 0.375\left(\frac{\pi}{M_4}\right)^{0.5} \tag{33}$$

The Gaussian distribution for the asperity heights is given as follows:

$$\Phi = \frac{(2\pi)^{-1/2}}{\sigma_s}\exp\left[-0.5\left(\frac{z}{\sigma_s}\right)^2\right] \tag{34}$$

McCool [45] defines σ_s to be the standard deviation of the asperity heights. This is calculated from the standard deviation of the entire surface (RMS roughness):

$$\sigma^2 = \sigma_s^2 + \frac{3.717\times10^{-4}}{\eta^2R^2} \tag{35}$$

For the GW case, the area and load are calculated using an integral of Φ and a function relating the z value to a value d. d is defined as the value above which the asperities will be in contact with the rigid flat. The compression distance, z–d, is the interference of the rigid flat with the asperity peaks and is known as ω for the remainder of this work.

$$A(d) = A_n\eta\int_d^\infty \bar{A}(\omega)\Phi(z)dz \tag{36}$$

$$P(d) = A_n\eta\int_d^\infty \bar{p}(\omega)\Phi(z)dz \tag{37}$$

For the perfectly elastic case, the $\bar{A}$ and $\bar{P}$ are acquired from the Hertz solutions given as:

$$\bar{A}_E = \pi R\omega \tag{38}$$

$$\bar{P}_E = \frac{4}{3}E'\sqrt{R}(\omega)^{3/2} \tag{39}$$

Furthermore, surface separation can be obtained by relating the distance from the mean surface height to the rigid flat, δ , to d.

$$\delta = d + y_s \tag{40}$$

The value y_s is defined by Front [46] as follows:

$$y_s = \frac{0.045944}{\eta R} \tag{41}$$

Appendix B. Statistical elastic plastic model

The statistical method calculates load and area as a function of separation instead of area as a function of load as seen in the multi-scale methods. Therefore, instead of using the critical force to define the elastic–plastic regime of contact, the critical interference is used. The critical interference value is given by [37] as follows:

$$\omega_c = \left(\frac{\pi CS_y}{2E'}\right)^2 R \tag{42}$$

For interference $\omega < 1.9\omega_c$, spherical contact is considered to effectively agree with the perfectly elastic Hertzian contact model. However, if $\omega \geq 1.9\omega_c$ then the following equations from JG are used in place of Eqs. (38) and (39). This substitution will provide the necessary values to calculate the elastic–plastic behavior of the asperities in contact.

$$\bar{A}_{JG} = \pi R\omega\left(\frac{\omega}{\omega_c}\right)^B \tag{43}$$

$$\bar{P}_{JG} = P_c\left\{\left[\exp\left(-\frac{1}{4}\left(\frac{\omega}{\omega_c}\right)^{5/12}\right)\right]\left(\frac{\omega}{\omega_c}\right)^{3/2} + \frac{4H_G}{CS_y}\left[1-\exp\left(-\frac{1}{25}\left(\frac{\omega}{\omega_c}\right)^{5/9}\right)\right]\frac{\omega}{\omega_c}\right\} \tag{44}$$

where

$$P_c = \frac{4}{3}\left(\frac{R}{E'}\right)^2\left(\frac{C}{2}\pi S_y\right)^3 \tag{45}$$

$$B = 0.14\exp(23e_y) \tag{46}$$

$$e_y = \frac{S_y}{E'} \tag{47}$$

$$\frac{H_G}{S_y} = 2.84 - 0.92\left(1-\cos\left(\pi\frac{a}{R}\right)\right) \tag{48}$$

$$\frac{a}{R} = \sqrt{\frac{\omega}{R}\left(\frac{\omega}{1.9\omega_c}\right)} \tag{49}$$

These equations are then used in Eqs. (36) and (37) for the single asperity area and load.

References

[1] J.A. Greenwood, J.B.P. Williamson, Contact of nominally flat surfaces, Proc. R. Soc. Lond. A (295) (1966) 300–319.
[2] W.R. Chang, I. Etsion, D.B. Bogy, An elastic-plastic model for the contact of rough surfaces, ASME J. Tribol. 109 (2) (1987) 257–263.

Please cite this article in press as: W.E. Wilson, et al., Surface separation and contact resistance considering sinusoidal elastic–plastic multi-scale rough surface contact, Wear (2009), doi:10.1016/j.wear.2009.07.012

[3] R.L. Jackson, I. Green, A statistical model of elasto-plastic asperity contact between rough surfaces, Tribol. Int. 39 (9) (2006) 906–914.
[4] L. Kogut, I. Etsion, A finite element based elastic-plastic model for the contact of rough surfaces, Tribol. Trans. 46 (3) (2003) 383–390.
[5] L. Kogut, R.L. Jackson, A comparison of contact modeling utilizing statistical and fractal approaches, ASME J. Tribol. 128 (1) (2005) 213–217.
[6] A. Majumdar, B. Bhushan, Fractal model of elastic-plastic contact between rough surfaces, ASME J. Tribol. 113 (1) (1991) 1–11.
[7] S. Wang, J. Shen, W.K. Chen, Determination of the fractal scaling parameter from simulated fractal regular surface profiles based on the weierstrass-mandelbrot function (IJTC2006-12068), in: STLE/ASME International Joint Tribology Conference 2006, San Antonio, TX, 2006.
[8] W. Yan, K. Komvopoulos, Contact analysis of elastic-plastic fractal surfaces, J. Appl. Phys. 84 (7) (1998) 3617–3624.
[9] C.K. Bora, et al., Multiscale roughness and modeling of MEMS interfaces, Tribol. Lett. 19 (1) (2005) 37–48.
[10] M. Ciavarella, et al., Linear elastic contact of the weierstrass profile, Proc. R. Soc. Lond. A 1994 (456) (2000) 387–405.
[11] R.L. Jackson, J.L. Streator, A multiscale model for contact between rough surfaces, Wear 261 (11–12) (2006) 1337–1347.
[12] N.A. Fleck, J.W. Hutchinson, A phenomenological theory for strain gradient effects in plasticity, J. Mech. Phys. Solids (41) (1993) 1825–1857.
[13] Y. Wei, J.W. Hutchinson, Hardness trends in micron scale indentation, J. Mech. Phys. Solids (51) (2003) 2037–2056.
[14] N.A. Fleck, et al., Strain gradient plasticity: theory and experiment, Acta Metall. Mater. 42 (2) (1994) 475–487.
[15] H. Gao, et al., Mechanism-based strain gradient plasticity-I, Theory. J. Mech. Phys. Solids (47) (1999) 1239–1263.
[16] H. Gao, et al., Mechanism-based strain gradient plasticity- II, Analysis. J. Mech. Phys. Solids (48) (2000) 99–128.
[17] J.F. Archard, Elastic, Deformation and the Laws of Friction, Proc. R. Soc. Lond. A 243 (1957) 190–205.
[18] M. Ciavarella, et al., Linear elastic contact of the Weierstrass Profile, Proc. R. Soc. Lond. A (456) (2000) 387–405.
[19] H.M. Westergaard, Bearing pressures and cracks, ASME J. of Appl. Mech. 6 (1939) 49–53.
[20] M. Ciavarella, et al., Elastic contact stiffness and contact resistance for the Weierstrass profile, J. Mech. Phys. Solids 52 (6) (2004) 1247–1265.
[21] M. Ciavarella, G. Murolo, G. Demelio, The electrical/thermal conductance of rough surfaces – the Weierstrass-Archard Multiscale Model, Int. J. Solids Struct. 41 (15) (2004) 4107–4120.
[22] Y.F. Gao, A.F. Bower, Elastic-plastic contact of a rough surface with Weierstrass profile, Proc. R. Soc. A 462 (2006) 319–348.
[23] Y.F. Gao, et al., The behavior of an elastic-perfectly plastic sinusoidal surface under contact loading, Wear 261 (2) (2006) 145–154.
[24] V. Krithivasan, R.L. Jackson, An analysis of three-dimensional elasto-plastic sinusoidal contact, Tribol. Lett. 27 (1) (2007) 31–43.
[25] R.L. Jackson, V. Krithivasan, W.E. Wilson, The pressure to cause complete contact between elastic plastic sinusoidal surfaces, IMechE J. Eng. Tribol. Part J. 222 (7) (2008) 857–864.
[26] W. Manners, Plastic deformation of a sinusoidal surface, Wear 264 (2008) 60–68.
[27] B.N.J. Persson, Elastoplastic contact between randomly rough surfaces, Phys. Rev. Lett. 87 (11) (2001) 116101.
[28] L. Pei, et al., Finite element modeling of elasto-plastic contact between rough surfaces, J. Mech. Phys. Solids 53 (11) (2005) 2385–2409.
[29] S. Hyun, et al., Finite-element analysis of contact between elastic self-affine surfaces, Phys. Rev. E 70 (2) (2004), pp. 026117-1–026117-12.
[30] M. Ciavarella, G. Delfine, G. Demelio, A "re-vitalized" Greenwood and Williamson model of elastic contact between fractal surfaces, J. Mech. Phys. Solids 54 (12) (2006) 2569–2591.
[31] A.W. Bush, R.D. Gibson, T.R. Thomas, The elastic contact of rough surfaces, Wear 35 (1975) 87–111.
[32] M. Ciavarella, G. Murolo, G. Demelio, On the elastic contact of rough surfaces: numerical experiments and comparisons with recent theories, Wear 261 (10) (2006) 1102–1113.
[33] J.F. Archard, Elastic deformation and the Laws of Friction, Proc. R. Soc. Lond. A (243) (1957) 190–205.
[34] M. Ciavarella, G. Demelio, Elastic multiscale contact of rough surfaces: archard's model revisited and comparisons with modern fractal models, J. Appl. Mech. 68 (3) (2001) 496–498.
[35] K.L. Johnson, J.A. Greenwood, J.G. Higginson, The contact of elastic regular wavy surfaces, Int. J. Mech. Sci. 27 (6) (1985) 383–396.
[36] K.L. Johnson, Contact Mechanics., Cambridge University Press, 1985.
[37] R.L. Jackson, I. Green, A finite element study of elasto-plastic hemispherical contact, ASME J. Tribol. 127 (2) (2005) 343–354.
[38] R. Holm, Electric Contacts, 4th ed., Springer Verlag, NewYork, 1967, 21.
[39] C.V. Madhusudana, Thermal Contact Conductance., Springer-Verlag, New York, 1996.
[40] M.G. Cooper, B.B. Mikic, M.M. Yovanovich, Thermal contact conductance, Int. J. Heat Mass Transfer (12) (1969) 279–300.
[41] R.L. Jackson, S.H. Bhavnani, T.P. Ferguson, A multi-scale model of thermal contact resistance between rough surfaces, ASME J. Heat Transfer 130 (2008) 081301.
[42] L. Kogut, I. Etsion, Electrical conductivity and friction fore estimation in compliant electrical connectors, STLE Tribol. Trans. 43 (4) (2000) 816–822.
[43] R.S. Prasher, P.E. Phelan, Microscopic and macroscopic thermal contact resistances of pressed mechanical contacts, J. App. Phys. 100 (2006).
[44] J.I. McCool, Comparison of models for the contact of rough surfaces, Wear (107) (1986) 37–60.
[45] B.W. Drinkwater, R.S. Dwyer-Joyce, P. Cawley, A study of the interaction between ultrasound and a partially contacting solid–solid interface, in: Mathematical, Physical and Engineering Sciences, The Royal Society, 1996.
[46] I. Front, The effects of closing force and surface roughness on leakage in radial face seals, in israel institute of technology, in: Technion, Israel Institute of Technology, Haifa, 1990.

Please cite this article in press as: W.E. Wilson, et al., Surface separation and contact resistance considering sinusoidal elastic–plastic multi-scale rough surface contact, Wear (2009), doi:10.1016/j.wear.2009.07.012